Hindawi
Mathematical Problems in Engineering
Volume 2022, Article ID 6452538, 10 pages
https://doi.org/10.1155/2022/6452538

Research Article

Stress Cone Effect Analysis and Optimum Design of Extra High-Voltage Cable Joint Using Neural Networks

Çağrı Köksal,[1] **Emrah Dokur**,[2,3] **and Aysel Ersoy**[1]

[1]*Department of Electrical Electronics Engineering, Istanbul University-Cerrahpasa, Istanbul 34320, Turkey*
[2]*Department of Electrical and Electronics Engineering, Bilecik Seyh Edebali University, Bilecik 11210, Turkey*
[3]*MaREI, The SFI Research Centre for Energy, Climate and Marine, University of College Cork, Cork, Ireland*

Correspondence should be addressed to Çağrı Köksal; cagrikoksal@ogr.iu.edu.tr

Received 4 October 2021; Revised 1 February 2022; Accepted 23 April 2022; Published 17 May 2022

Academic Editor: Dragan Poljak

The major problem in high-voltage cable accessories is the electric field stress caused by the high-voltage level at the cable junction. In this paper, a neural network and simulation-based optimal design for extra high-voltage (EHV) cable accessory is proposed to ensure the optimum electrical design. The different kinds of geometries of the EHV underground cable accessory are realized in the Comsol Multiphysics software program, and the electric field analyses are conducted based on the finite element method. The design of high-voltage underground cable accessories is examined both within and without the optimal stress cone geometry. A neural network-based model is developed according to the analysis results obtained in the simulation. Thanks to this model, the geometry of the stress cone is determined. In the simulation-based analysis, the electric field stress caused by the high-voltage level at critical points is controlled with an optimum joint design using neural networks. The proposed model will contribute to EHV cable joint design at different stress levels.

1. Introduction

A higher capacity transmission path is required to satisfy the power demand of the society having a steady increase in electricity consumption. Installing high-voltage cables is an inevitable trend in metropolitan areas and densely populated areas.

High-voltage underground cables are manufactured in limited length due to obstacles seen during production and transportation. High-voltage cable accessories and cables that have limited length are combined to ensure the continuity of the power line. With the rapid growth of installation of high-voltage underground cables, cable failure faults frequently occur in large cities due to the unqualified accessories installation and unusual external operating environment [1–3]. According to the statistics of cable failures in the last 10 years, the share of cable accessory failure is more than half of the total cable defect. Among the power cable failures in gird, more than 75% of cable failures occur in the conventional cable joint without considering the failures caused by the external destruction [4, 5]. The major problem in high-voltage cable accessories is the electric field stress caused by the high-voltage level at the cable junctions [6]. Generally, the high-voltage accessories are the most sensitive parts and are in danger of failure in the cable system [7–9]. The reliability of cable is related to its accessories such as joints and terminations since they have a much higher failure rate than the cable itself [10]. The weaknesses of cable accessories are correlated to the nonuniform distribution of their internal electric field [11].

It is necessary to know the distribution of electric field intensity and especially its value in the places where it is the highest for high-voltage underground cables [12–14]. As the energy transmission system voltage increases, due to load conditions and development, the insulation must operate under greater electrical stresses. For this reason, using a larger-sized insulation material does not give good results as it will make the device heavier and increase the thermal impedance. It is necessary (i) to control the excessive electric field stresses that may occur on the high-voltage cable screen and (ii) to reduce the electric field stress in the critical region [15].

The historical development of stress control is given in Figure 1. The impedance stress control based on heat-shrinkable tubing and nonlinear stress control were used in these developments [16].

Originally, some researchers approximating and modelling elastic continua using discrete equivalent elastic bars in the early 1900s proposed the finite element method [17]. However, Courant presented and developed the modern finite element method in 1940. Piecewise polynomial interpolation over triangular subregions was used by Courant to research torsion problems. The next important step in the utilization of finite element methods was taken by Boeing in the 1950s by using triangular stress elements to model airplane wings. In 1960, Clough made the term "finite element" popular, and during the 1960s, investigators began to apply the finite element method to other areas of engineering, such as heat transfer and seepage flow problems. The first book about the finite element method was written in 1967 by Zienkiewicz and Cheung [18].

In the open literature, there are many studies for electric field stress control in high-voltage underground cables [7, 19–22]. Yang et al. [12] conducted comparative analyses on the evaluation of contact resistance of simulation-based cable joints. Letvenuk et al. [23] examined the air gap effect for medium voltage cable accessories. They proposed a new material-based approach to control stress levels. Frobin et al. [24] presented a Comsol Multiphysics software-based general approach for the modelling of HVDC cable accessories. Hyperelastic material-based cable accessories were designed by Luo et al. [25]. Electric field distributions of stress cones were analysed using a material with nonlinear conductivity [26]. The electric field distribution inside the cable accessories can be improved by adjusting the curvature and axial length of the stress cone [27, 28]. Although there are empirical approaches to optimum design in the studies, it is seen that an AI-based general approach is not presented.

The most important component of the joints the stress cone is used for the reduction of the maximum electric field stress, which is concentrated at the critical point where the screen ends during cable joining. This paper aims to compare and analyse the stress cone effect according to two different cases which are with stress cone and without stress cone structure firstly. Afterwards, an artificial neural network model was created according to the simulation results. Thus, the optimum stress cone was designed using this model. All analyses were performed by a simulation-based method for the 500 kV high-voltage accessories.

The paper is organized as follows. The design of the EHV joint based on a neural network is presented in Section 2. The geometry of the proposed model is given in Section 3. All analysis results are presented and discussed in Section 4. The conclusion is given in Section 5.

2. Neural Network-Based Optimal Design of EHV Joint

Insulating materials in the electric field are forced by the effect of this field. Electrical stress may cause surface discharge or breakdown of the insulator. To minimize the risk

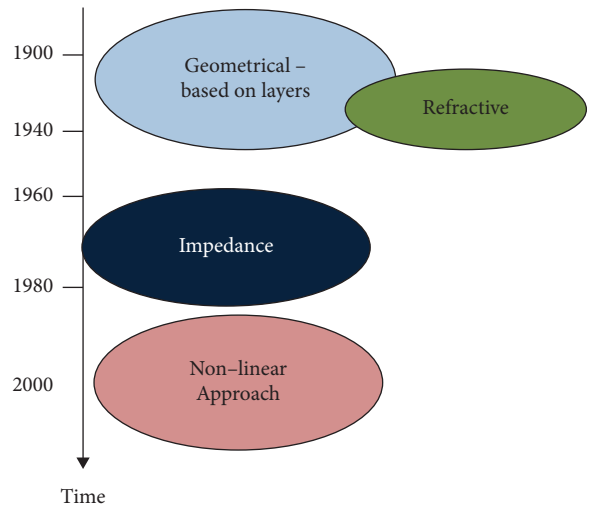

Figure 1: Development of electric stress control.

of superficial discharge or puncture and to get the most efficient result from electrode systems, the insulating material should be forced equally everywhere, and a uniform electric field distribution on the electrode surface should be provided.

The electrical stress in critical areas of high-voltage cable joints has to be reduced at the design stage. Partial discharge (PD) can occur due to high electric field intensity in different critical areas of the cable joint. After the partial PD starts, treeing occurs, and then, the structure causing more PD appears. This will cause an acceleration in the aging procedure. Design failures, installation, and manufacturing process-related defects can cause PD to occur in the cable connection. Under 132 kV and above the HV level of joints, PD is very crucial at the design stage [19].

In this study, the focus is on reducing the electric field in critical areas by using a stress cone. If the electric potential is known at every point in a region of space, the electric field can be derived from the potential. The electric field intensity is obtained from the negative gradient scalar potential. The relationship equation of electric field $\vec{E}$ and potential function V is given as follows:

$$\vec{E} = -\nabla V. \tag{1}$$

The tangential component of the electrical field is continuous across the surfaces separating two different materials. Hence, the potential function V is continuous everywhere in the domain. From the Ampere–Maxwell equation,

$$\nabla \cdot \vec{J} + \frac{\partial (\nabla \cdot \vec{D})}{\partial t} = 0, \tag{2}$$

where the conduction current density represents as $\vec{J}$ and $\vec{D}$ is the electric displacement.

We assume the following as initial conditions:

$$\nabla \cdot \vec{D} = 0 \text{ at } t = 0. \tag{3}$$

That is, at $t = 0$, there is no free charge in the system. The electric displacement in linear isotropic materials is simply involved in the electric field as follows:

$$\vec{D} = \varepsilon \vec{E}, \tag{4}$$

where ε is the permittivity measured in farads per meter (F/m). The coefficient ε can be written as

$$\varepsilon = \varepsilon_0 \varepsilon_r, \tag{5}$$

where ε_0 (F/m) is the permittivity of free space and ε_r is the relative permittivity of the medium. The current density and the electric field are related to a complex relationship in nonlinear materials.

$$\vec{J} = \sigma(E)\vec{E}, \tag{6}$$

where a field-dependent conductivity represents as $\sigma(E)$. In the nonconducting regions, such as in all regular points, from equations (l), (3), and (4), it follows that the Laplace equation for the potential holds

$$\nabla \cdot \left(-\varepsilon_0 \varepsilon_r \nabla V\right) = 0. \tag{7}$$

In the nonlinear regions, that is, in all regular points, from equations (l)–(4) and (6), it follows that the dynamics of the electric potential is described by a nonlinear diffusion like equation [29].

$$\nabla \cdot \left[-\sigma(\vec{E})\nabla V\right] = \frac{\partial}{\partial t}\left[\nabla \cdot \left(\varepsilon_0 \varepsilon_r (\vec{E})\nabla V\right)\right]. \tag{8}$$

By applying the backward Euler method, the problem is discretized, and (8) becomes the following equation:

$$\nabla \cdot \left[-\left(\sigma(\vec{E}) + \frac{\varepsilon_0 \varepsilon_1}{\Delta t}\right)\nabla V(t)\right] = -\varepsilon_0 \varepsilon_r \frac{\nabla^2 V(t - \Delta t)}{\Delta t}, \tag{9}$$

where t is the time, and it is a suitable small time interval [30].

A cross-sectional view of a typical 500 kV cable joint is shown in Figure 2.

The peak stress at the cable outer semicone cutting point can be controlled by the optimal stress cone curvature. (a) On the other hand, the peak stress inside the cable joint body can be regulated by the cage tip curvature, (b) which is one of the most important design parameters. The surface stress and surface flashover are affected by the distance between the cage and the stress cone. (c) The insulation thickness (d) between the joint cage and the outer ground layer needs to withstand the highest average stress. This area is similar to a parallel plate configuration. From the electrostatic model, it is clear that the most crucial path will be near the joint cage tip. The axial and radial electric fields can generally be calculated from equations (9) and (10) [20].

$$\begin{aligned} E_{\text{axial}}(l, r) &= -U_n \cdot \frac{C_n}{2\pi\varepsilon} \frac{1}{lr} \frac{\partial r}{\partial l}, \\ E_{\text{radial}}(l, r) &= U_n \cdot \frac{C_n}{2\pi\varepsilon} \cdot \frac{1}{lr}, \end{aligned} \tag{10}$$

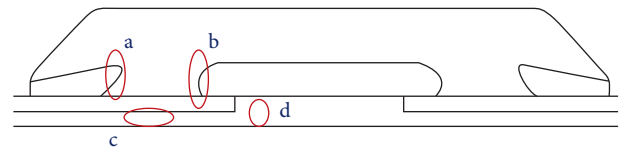

Figure 2: Critical areas of the HV cable joint.

where the length of each conductive layer is l, r is the distance between the conductive layer and screen cut, ε is the permittivity of the surrounding insulating material, and U_n is the voltage between each layer.

The electric field strength E of each layer depends on the voltage U, length l, radial distance r, and permittivity ε as shown in the following equation:

$$E(l, r) = \frac{U}{r_n l_n \varepsilon_{rn} \sum_{n=1}^{n} \ln\left(r_{n+1}/r_n\right)/l_n \varepsilon_n}. \tag{11}$$

The electric field is one of the most important factors for the optimum sizing of EHV joints. Methods in which the electrode shape is iterated to achieve the desired area distribution [31–35] are not effective for many problems. Since the area must be calculated in every iteration, the calculation time is quite long. Besides being time-consuming, these methods cannot always provide a general solution.

In this paper, such an optimization problem is solved using a multilayer feed-forward neural network algorithm (Figure 3). The neural network is trained to obtain a stress cone profile that will provide the desired area distribution on the joint surface. The analysis data are divided into a 70 : 30 ratio after normalization. 70% of data are employed for training the model, and the remaining 30% data are utilized for testing the performance of the model. The proposed neural network consists of three hidden layers. In this study, 10 neurons are used in hidden layers. Also, the Levenberg-Marquardt learning function is used for training. All results of the neural network model are given in Section 4 detailed.

Neural network-based models are run separately 100 times, and the results are presented statistically to eliminate the errors that may arise from the randomness of the model parameters. The performance of model is evaluated by considering the deviation of the predicted value from the target value. For this purpose, the root mean square error (RMSE), mean square error (MSE), and mean absolute error (MAE) are used. The performance metrics are mathematically represented in (12) through (14) as follows:

$$RMSE = \sqrt{\frac{\sum_{i=1}^{N} \left(y_i - \tilde{y}_i\right)^2}{N}}, \tag{12}$$

$$MSE = \frac{\sum_{i=1}^{N} \left(y_i - \tilde{y}_i\right)^2}{N}, \tag{13}$$

$$MAE = \frac{\sum_{i=1}^{N} \left|y_i - \tilde{y}_i\right|}{N}, \tag{14}$$

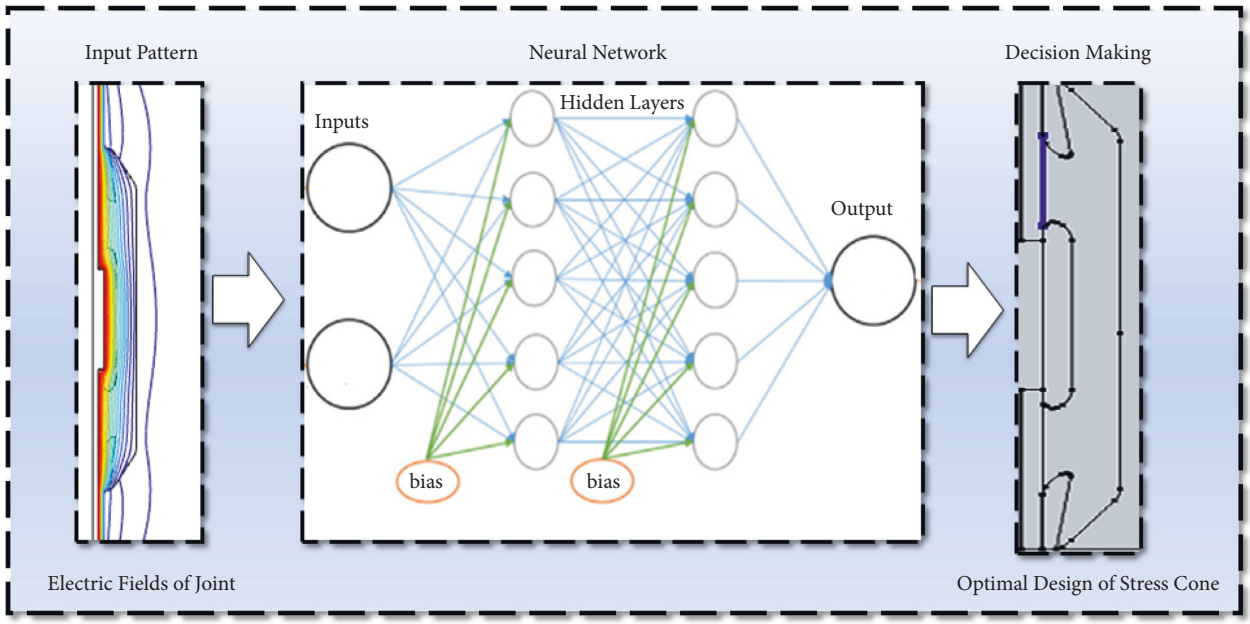

Figure 3: The flowchart of neural network structure.

where yi and $\tilde{y}_i$ represent the observed value and predictive value of the model and N is the total number of data used for performance evaluation and comparison.

3. Geometry of the Proposed Model

The geometries of the high-voltage underground cable accessories have been realized in the Comsol Multiphysics software program, and the electric field analyses have been conducted based on the finite element method (FEM). For electric field simulations using FEM, COMSOL Multiphysics software is a complete platform for simulating variations in the power cables. For the FEM analysis, an object is divided into equal parts, and based on the equations, each element's behavior is forecasted. Thanks to this method, all individual behaviors are analysed and added, thus obtaining the object's total behavior resulting from the sum of each element. With the sum of the elements, a mesh is obtained, which can have variations that result in greater accurate and computational cost, depending on the configuration used. There are several ways to determine each element, which are subdivided for mathematical evaluation. In this paper, the triangular shapes on the boundary are used for mesh. The number of finite element and boundary element is designed as 53066 and 2083, respectively. The computational time of the analyses is three seconds. The operations that will be applied when a problem is solved with a finite element package software COMSOL are given as follows:

(i) The problem is geometrically plot

(ii) Materials and properties of the region are defined for the geometry

(iii) Boundary conditions for the problem are identified

(iv) The geometry is divided into smaller subregions, and equations for these subregions are defined according to the boundary conditions by the software

(v) The mathematical model is solved by the package software by considering all the stated conditions

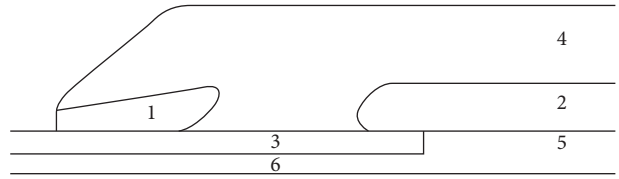

Figure 4: The cable joint geometry. (1) Stress cone; (2) middle electrode; (3) cable insulation (XLPE); (4) joint insulation (EPDM); (5) connector; (6) conductor.

Table 1: 500 kV HV cable information.

Cable dimensions	
Size (mm^2)	2500
Diameter (mm)	63,5
Thickness of insulation (mm)	30
Thickness of conductive screen (mm)	1,6

Stress cone design in joint geometry for 500 kV high-voltage underground cables analysed in Comsol Multiphysics program. The design of high-voltage underground cable accessories has been examined for different stress cone geometries and without stress cones. In addition, different conditions for joint design have been analysed comparatively. The joint used in the simulation is an ethylene propylene diene monomer (EPDM) filled flat connection for 500 kV crosslinked polyethylene (XLPE) cables. Figure 4 shows the joint geometry and part of the joint.

Information about the cable used in the simulation is given in Table 1.

Table 2: Material parameters for 500 kV EHV cable joint [26].

Material	Relative permittivity	Conductivity (S/m)
Cable core	1	5.7×10^7
Semiconductive stress cone	50	10
XLPE	2.3	10^{-15}
Nonlinear material	4.3	$\sigma = f(\mathrm{E})$
EPDM	2.6	10^{-15}
Semiconducting middle electrode	50	10

The properties of the cable insulation system consisting of insulation materials used in the joint design are presented in Table 2.

These materials have been selected to keep the maximum electric field stress under control. The AC voltage test specification states that the cable joints should be tested at 2.5 U0 for 15 minutes with no breakdown. In this paper, 1550 kV impulse voltage has been applied in the joint. The 3D voltage profile of the proposed model is given in Figure 5.

4. Simulation Results and Effect of Stress Cone Design

During cable joint production, stress control is concentrated in areas where the cable screens are peeled off. Design is important for these regions. The contour plot of the voltage profile in the joint is given in Figure 6. Electric field stress control is carried out by means of the middle electrode in the connector area and the stress cone.

The joint designs without stress cones are shown in Figure 7. Here, the critical regions must be determined from the electric field distribution in the direction of the z component. The electric field distribution in the region indicated by the red line is given in Figures 7 and 8.

It is observed that the electric field value reaches approximately 34 kV/mm in critical regions. Reducing this value in critical areas is essential for component safety. In this case, along with the deformation of the insulation, failure will occur as a result of partial discharge and breakdown. Even if increasing the size of the insulation material allows the electric field to be reduced in these areas, this is not an effective approach. Therefore, an optimal stress cone design can provide stress control in this region. The joint structure with stress cone analysed is shown in Figure 9.

Using the stress cone, the highest stress can be seen to be approximately 21 kV/mm at the critical region of the joint (Figure 10).

Stress cone is the most important component of the joint, which reduces the maximum electric field stress that condenses at the critical point where the screen ends during cable jointing, thus preventing partial discharge and insulation problems. In the analyses, the electric field value in the critical region has been reduced using the neural network-based optimal stress cone design. Additionally, the effect of joint geometry on the tangential electric field strength in material interfaces is shown in the analysis.

While determining the optimum stress cone design, the effect of the distance between the stress cone and the middle electrode, which is one of the most important parameters, on the electric field distribution in critical regions was investigated (Table 3). The variation of the electric field values (in different regions as shown in Figure 11) according to the distance between the middle electrode and the stress cone was examined.

In Figure 11, A is the outer stress cone, curvature, side electrode, or semiconductive deflector. B shows the distance between the stress cone and the middle electrode. Middle electrode, EHV deflector, Faraday cage, or inner stress cone are presented by C. Stress cone and cable insulation interface are indicated with D. As it can be seen from Table 3, the electric fields in different regions are determined by

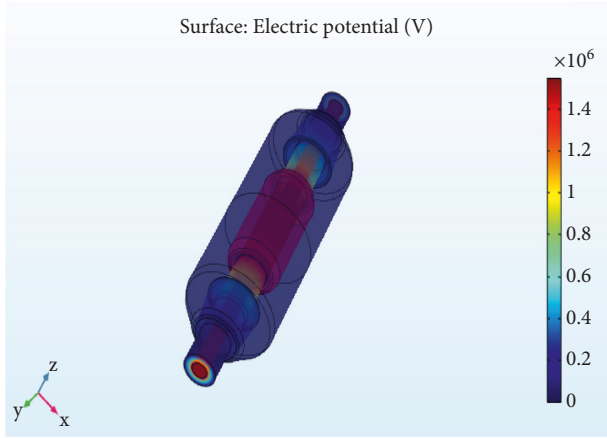

Figure 5: 3D view of the cable joint and voltage profile.

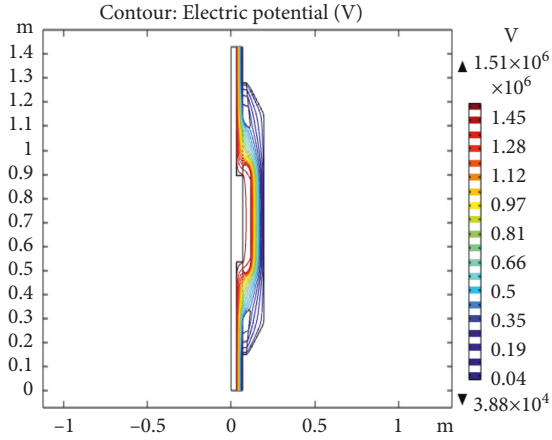

Figure 6: Voltage profile of the cable joint.

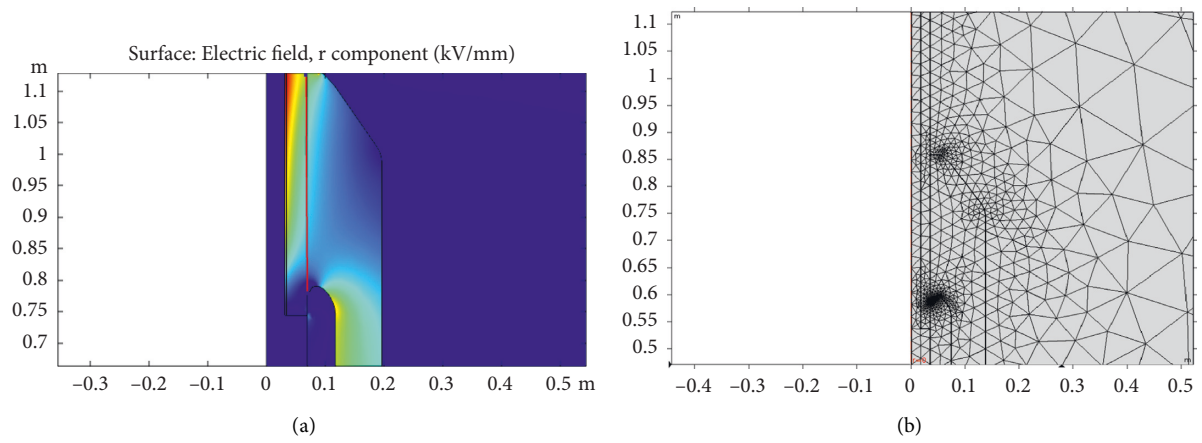

Figure 7: Critical region of the joint without stress cone. (a) Mesh grid. (b) Electric field density.

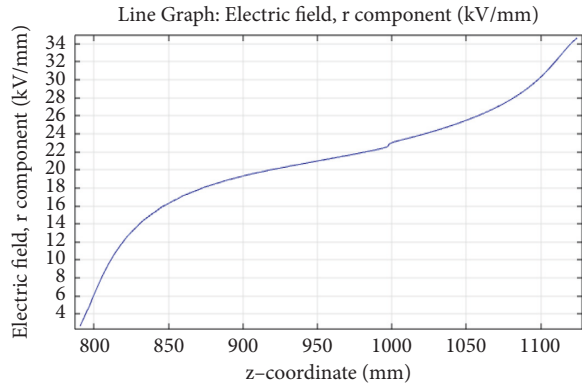

Figure 8: Electric field z component of the joint without stress cone.

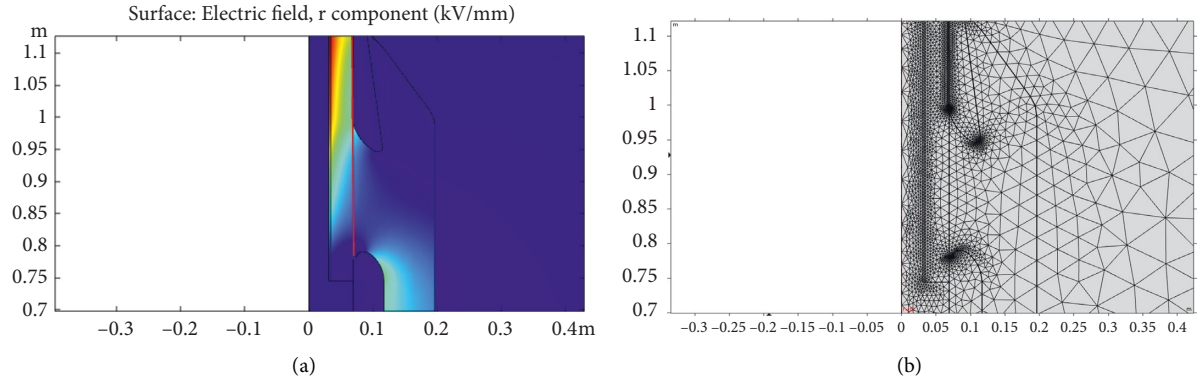

Figure 9: Critical region of the joint with stress cone. (a) Electric field density. (b) Mesh of the cable joint.

increasing the electrode length by 2 cm intervals for each design scenario. While the electric field in different regions constitutes the input vector of artificial neural networks, the output vector is the distance between the stress cone and the middle electrode.

The neural network-based model was run 100 times, and the best, worst, average, and standard deviation (Std) values of the error performance criteria are shown in Table 4. After the training and testing are completed, the artificial neural network gives the optimal distance to the desired electric field values.

Considering the permissible electric field levels in critical regions for a 500 kV joint, the joint number 5 is obtained in the model created in the neural network. The created model will contribute to the decision-making at different voltage levels.

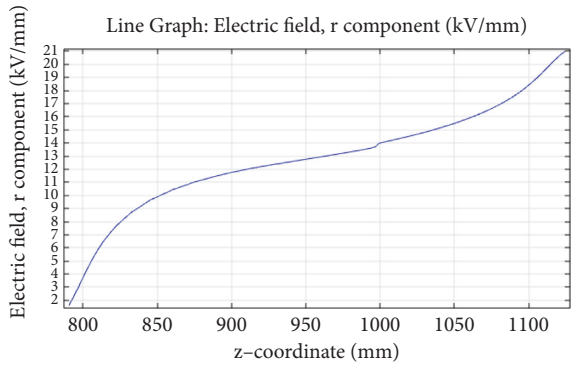

Figure 10: Electric field z component of the joint with stress cone.

Table 3: Electric field changes according to different geometries.

Joint number	Stress cone-middle electrode (cm)	Electric fields (kV/mm)						
		A	B	C	D	$z=0$ E $r=31$ cm	F $r=67$ cm	G $r=91$ cm
1	24	9.355	23.466	12.470	19.985	30.114	35.693	0.209
2	22	9.347	23.443	12.504	19.998	30.092	35.705	0.211
3	20	9.335	23.410	12.493	20.008	30.087	35.724	0.210
4	18	9.333	23.362	12.639	20.028	30.079	35.751	0.211
5	16	9.321	23.304	12.562	20.060	30.069	35.788	0.214
6	14	9.299	23.226	12.597	20.102	30.073	35.829	0.214
7	12	9.277	23.111	12.727	20.159	30.053	35.900	0.217
8	10	9.245	22.951	12.740	20.243	30.026	36.004	0.221
9	8	9.227	22.715	12.905	20.356	29.968	36.154	0.226
10	6	9.165	22.375	12.938	20.529	29.924	36.374	0.234
11	4	9.083	21.818	12.950	20.819	29.808	36.731	0.247
12	2	9.624	20.765	13.148	21.336	29.643	37.378	0.272

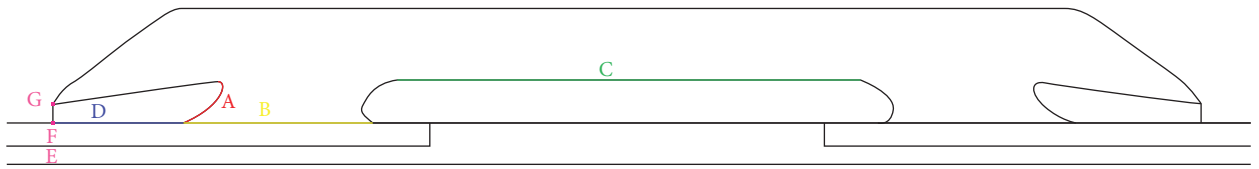

Figure 11: The joint regions used in the data set for the neural network model.

Table 4: Comparison of model training and test results with 100 independent runs.

	Training			Test		
	RMSE	MSE	MAE	RMSE	MSE	MAE
Best	1.57e−03	2.46e−06	1.07e−03	1.41e−02	1.98e−04	1.12e−02
Worst	8.09e−02	6.55e−03	6.68e−02	2.14e−01	4.58e−02	2.13e−01
Mean	1.48e−02	4.20e−04	1.10e−02	1.07e−01	1.31e−02	9.25e−02
Std.	1.42e−02	9.58e−04	1.24e−02	4.09e−02	9.27e−03	3.71e−02

Silicone rubber semiconductor and conductive components designed according to the geometric stress control method have been designed with iterative steps until all desired ambient conditions. It has been predefined to achieve the desired final accessory design using the neural network model.

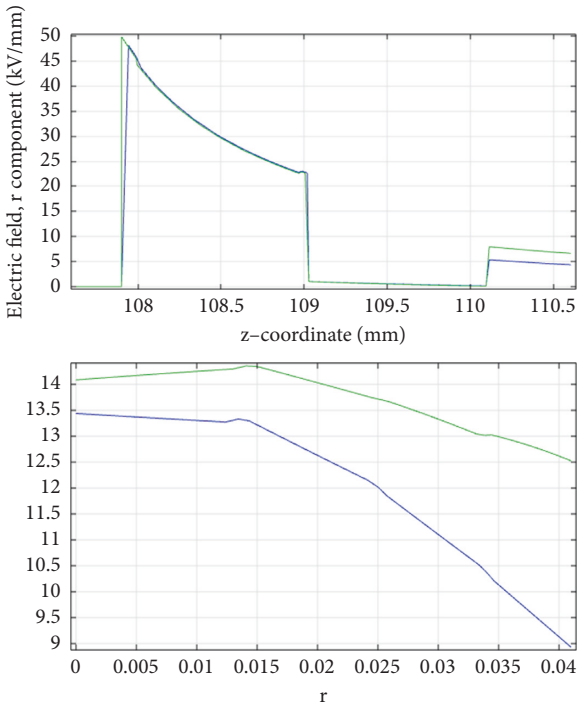

Figure 12: The joint regions used in the data set for the neural network model.

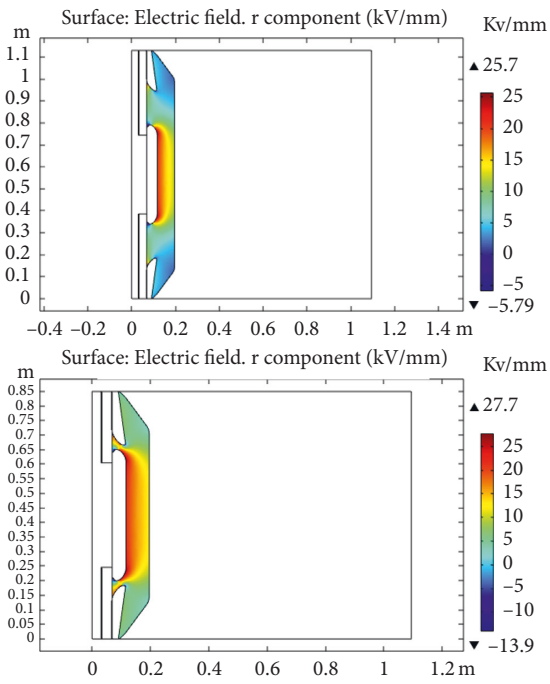

Figure 13: Electric field variations in different regions for joint numbers-5 and 12.

Electric field distribution was obtained with the optimal model blue line (joint number 5) and joint number 12; that is, the green line for different regions is also presented in Figure 12.

The electric field distribution on the EPDM surface is shown in Figure 13 for both scenarios (joint numbers 5 and 12).

It is seen that the electric field distribution in Figure 12 for the optimal model (joint number 5) that was found by the neural network model in the region where EPDM is located remains within the allowable limits as stated in the literature [36].

5. Conclusion

The optimal joint design has become increasingly important with the widespread use of cables at extra high-voltage levels. One of the most important components in the joint design is the creation of an optimal stress cone structure. Especially, determining and decreasing the area of the highest electric field on the joint is an important factor in terms of partial discharges.

In this paper, the electric field stress created by the high-voltage level at critical points has been kept under control with the appropriate joint design via simulation and neural network-based optimization. The use of stress cone configuration reduces the maximum electric field strength inside the EHV joint. The use of the stress cone has been successful in controlling the maximum electric field in the joint design. However, the distance of the stress cone to the middle electrode is an important problem in the design. A neural network-based model is used to solve this problem. In this way, the electric fields in different critical regions are optimized with the neural network-based stress cone design. Model performance with 12 different scenarios is shown comparatively in this paper. In the results obtained, choosing the distance between the stress cone and the middle electrode as 16 cm is the most appropriate value for a 500 kV joint.

This initial phase of the study will continue with the experimental verification of the optimal design.

Data Availability

The neural network and joint data used to support the findings of this study are available from the corresponding author upon request.

Conflicts of Interest

The authors declare that they have no conflicts of interest.

Acknowledgments

The authors would like to thank the Manager of Demirer Cable Accessories Design Department, Enis TUNA, for his help in simulation models.

References

[1] C.-K. Chang, C.-S. Lai, and R.-N. Wu, "Decision tree rules for insulation condition assessment of pre-molded power cable joints with artificial defects," *IEEE Transactions on Dielectrics and Electrical Insulation*, vol. 26, no. 5, pp. 1636–1644, 2019.

[2] H. Yang, L. Liu, K. Sun, and J. Li, "Impacts of different defects on electrical field distribution in cable joint," *Journal of Engineering*, vol. 2019, no. 16, pp. 3184–3187, 2019.

[3] W. J. K. Raymond, H. A. Illias, and A. H. Abu Bakar, "High noise tolerance feature extraction for partial discharge classification in XLPE cable joints," *IEEE Transactions on Dielectrics and Electrical Insulation*, vol. 24, no. 1, pp. 66–74, 2017.

[4] J. H. He, K. He, and L. F. Cui, "Charge-simulation-based electric field analysis and electrical tree propagation model with defects in 10 kV XLPE cable joint," *Energies*, vol. 12, no. 23, Article ID 4519, 2019.

[5] L. Zhang, X. LuoYang, Y. Le, F. Yang, C. Gan, and Y. Zhang, "A thermal probability density-based method to detect the internal defects of power cable joints," *Energies*, vol. 11, no. 7, Article ID 1674, 2018.

[6] B. Akbal, "MSSB to prevent cable termination faults for long high voltage underground cable lines," *Elektronika ir Elektrotechnika*, vol. 25, no. 6, pp. 8–14, 2019.

[7] H. Ye and T. X. Y. M. Z. H. Q. R. D. Fechner, "Review on HVDC cable terminations," *High Voltage*, vol. 3, no. 2, pp. 79–89, 2018.

[8] F. Rahmani, D. Quispe, T. Agarwal, and M. Barzegaran, "Speed control of brushless DC motor by DC-DC boost and buck converters using GaN and SiC transistors for implementing the electric vehicles," *Brushless DC Motors*, vol. 6, pp. 70–75, 2020.

[9] P. Dehghanian, K. S. Shetye, K. R. Davis, and T. J. Overbye, "System-wide case study assessment of transformer heating due to geomagnetic disturbances," in *Proceedings of the 2019 North American Power Symposium (NAPS)*, pp. 1–6, Wichita, KS, USA, October 2019.

[10] S. Hou, M. Fu, C. Li, B. Han, C. Zhang, and Z. Li, "Electric field calculation and analysis of HVDC cable joints with nonlinear materials," in *Proceedings of the 2015 IEEE 11th ICPADM*, pp. 184–187, Sydney, July 2015.

[11] J. Su, B. Du, J. Li, and Z. Li, "Electrical tree degradation in high-voltage cable insulation: progress and challenges," *High Voltage*, vol. 5, no. 4, pp. 353–364, 2020.

[12] F. Yang, K. Liu, P. Cheng et al., "The coupling fields characteristics of cable joints and application in the evaluation of crimping process defects," *Energies*, vol. 9, no. 11, p. 932, 2016.

[13] E. Kantar, D. Panagiotopoulos, and E. Ildstad, "Factors influencing the tangential AC breakdown strength of solid-solid interfaces," *IEEE Transactions on Dielectrics and Electrical Insulation*, vol. 23, no. 3, pp. 1778–1788, 2016.

[14] T. Liu, B. Hui, M. Fu, S. Hou, B. Luo, and G. Wang, "Experimental and simulation analysis of electrical breakdown for 220kV silicone rubber pre-moulded cable joints," in *Proceedings of the 13th International Electrical Insulation Conference*, Birmingham, May 2017.

[15] F. A. M. Rizk and G. N. Trinhhigh, *High Voltage Engineering, CRC Press, Boca Raton, FL, USA*, 2018.

[16] M. Abdel-Salam, "High-voltage engineering: theory and practice," *Revised and Expanded*, 2018.

[17] S. Das, B. Pandyan, and P. Bhugra, "Robust high voltage cable joint design," in *Proceedings of the 2015 IEEE IAS Joint Industrial and Commercial Power Systems/Petroleum and Chemical Industry Conference (ICPSPCIC)*, Hyderabad, India, November 2015.

[18] O. C. Zienkiewicz and Y. K. Cheung, *The Finite Element in Structural and Continuum Mechanics, Mcgraw-Mill Puolishing Company Limited, New York, NY, USA*, 1967.

[19] S. Li and J. Li, "Condition monitoring and diagnosis of power equipment: review and prospective," *High Voltage*, vol. 2, no. 2, pp. 82–91, 2017.

[20] A. Eigner and S. Semino, "50 years of electrical-stress control in cable accessories," *IEEE Electrical Insulation Magazine*, vol. 29, no. 5, pp. 47–55, 2013.

[21] A. F. Andrade, E. G. Costa, F. L. M. Andrade, C. S. H. Soares, and G. R. S. Lira, "Design of cable termination for AC breakdown voltage tests," *Energies*, vol. 12, no. 16, 3075 pages, 2019.

[22] T. Sun, Y. Zhang, X. Guo, and Y. Xu, "Partial discharge behavior of 220 kV prefabricated cable termination induced by inadequate interface pressure," in *Proceedings of the 2018 12th International Conference on the Properties and Applications of Dielectric Materials (ICPADM)*, Xi'an, China, May 2018.

[23] M. Letvenuk, M. Beninca, H. Noglik, and P. Sheridan, "The use of shear responsive stress control mastics as void fillers in medium voltage cable accessories," *IEEE Electrical Insulation Magazine*, vol. 33, no. 2, pp. 16–23, 2017.

[24] J. Frobin, C. F. Niedik, C. Freye, J. Frank, D. Häring, and G. Schröder, "Generic approach for HVDC cable accessories modelling," in *Proceedings of the IEEE 2nd International Conference on Dielectrics (ICD)*, Budapest, Hungary, July 2018.

[25] Y. Luo, Z. Han, X. Lei et al., "Techniques for designing prefabricated cable accessories based on hyperelastic material model," in *Proceedings of the 12th IEEE International Conference on the Properties and Applications of Dielectric Materials*, pp. 987–991, China, May 2018.

[26] X. Zhao, X. Yang, L. Gao, Q. Li, J. Hu, and J. He, "Tuning the potential distribution of AC cable terminals by stress cone of nonlinear conductivity material," *IEEE Transactions on Dielectrics and Electrical Insulation*, vol. 24, no. 5, pp. 2686–2693, 2017.

[27] H. Ghorbani, M. Jeroense, C. O. Olsson, and M. Saltzer, "HVDC cable systems-highlighting extruded technology," *IEEE Transactions on Power Delivery*, vol. 29, no. 1, pp. 414–421, 2014.

[28] T. Christen, L. Donzel, and F. Greuter, "Nonlinear resistive electric field grading part 1: theory and simulation," *IEEE Electrical Insulation Magazine*, vol. 26, no. 6, pp. 47–59, 2010.

[29] C. Petrarca, D. Cerbasi, V. Tucci, and M. Vitelli, "Numerical analysis of performances of stress grading cable accessories made of different anisotropic composite materials," in *Proceedings of the 2000 Annual Report Conference on Electrical Insulation and Dielectric Phenomena (Cat. No.00CH37132)*, vol. 2, pp. 494–497, Victoria, BC, Canada, October 2000.

[30] L. Egiziano, V. Tucci, C. Petrarca, and M. Vitelli, "A Galerkin model to study the field distribution in electrical components employing nonlinear stress grading materials," *IEEE Transactions on Dielectrics and Electrical Insulation*, vol. 6, no. 6, pp. 765–773, 1999.

[31] W. M. Caminhas, R. R. Saldanha, and G. R. Mateus, "Optimization methods used for determining the geometry of shielding electrodes," *IEEE Transactions on Magnetics*, vol. 26, no. 2, pp. 642–645, 1990.

[32] C. Trinities, "Accelerated 3-D optimization of high voltage apparatus," in *Proceedings of the The Ninth International Symposium on High Voltage Engineering*, Graz, Austria, August 1995.

[33] K. Kato, M. Hikita, N. Hayakawa, and H. Okubo, "High efficient method for determination of electric field optimum contour of high voltage electrode," in *Proceedings of the The*

Ninth International Symposium on High Voltage Engineering, Graz, Austria, August 1995.

[34] K. Kato and H. Okubo, "Optimization of HV electrode contour with the highest gaseous insulation performance," *IEEE Transactions on Dielectrics and Electrical Insulation*, vol. 4, no. 6, pp. 816–821, 1997.

[35] K. Kato, X. Han, and H. Okubo, "Insulation optimization by electrode contour modification based on breakdown area/volume effects," *IEEE Transactions on Dielectrics and Electrical Insulation*, vol. 8, no. 2, pp. 162–167, 2001.

[36] T. Sheta, A. H. Gad, L. S. Nasrat, and S. M. El-Debeiky, "Evaluation of dielectric strength of epdm elastomer loaded with ath filler," *International Journal of Engineering Science Technologies*, vol. 4, no. 3, pp. 13–18, 2020.